PERGAMON

International Journal of Heat and Mass Transfer 45 (2002) 4695–4702

International Journal of HEAT and MASS TRANSFER

www.elsevier.com/locate/ijhmt

Solutocapillary convection in the float-zone process with a strong magnetic field

J.S. Walker [a,*], P. Dold [b], A. Cröll [c], M.P. Volz [d], F.R. Szofran [d]

[a] *Department of Mechanical and Industrial Engineering, University of Illinois, 1206 West Green Street, Urbana, IL 61801, USA*
[b] *Kristallographisches Institut, University of Freiburg, Hebelstr. 25, D-79104 Freiburg, Germany*
[c] *Institut für NE-Metallurgie und Reinststoffe, Technical University of Freiberg, Leipziger Str. 23, D-09599 Freiberg, Germany*
[d] *SD 47, NASA Marshall Space Flight Center, Huntsville, AL 35812, USA*

Received 15 February 2001; received in revised form 7 July 2001

Abstract

This paper treats the steady axisymmetric flow and mass transport in a cylindrical liquid bridge between the melting end of a feed rod and the solidifying end of an alloyed semiconductor crystal. There is a strong, uniform, steady, axial magnetic field. The surface tension depends on the temperature and the concentration of the species, while variations of the concentration occur because one species is rejected into the liquid during solidification. The thermocapillary and solutocapillary convections tend to cancel over part of the liquid bridge. For certain parameter ranges, there are two different stable solutions: one where the concentration gradient along the free surface leads to dominance by the solutocapillary convection and one where the mass transport due to the thermocapillary convection makes the concentration gradient along the free surface small, so that the thermocapillary convection is dominant.

1. Introduction

In the float-zone crystal-growth process, a liquid bridge with a roughly cylindrical free surface is held by surface tension between the melting bottom end of a vertical, cylindrical feed rod and the solidifying top end of a coaxial, vertical, cylindrical crystal. A heat flux into the free surface keeps the liquid temperature above the solidification temperature T_s^*. The free-surface temperature varies from a maximum of $T_s^* + (\Delta T^*)$ at a circumference roughly midway between the feed rod and crystal to T_s^* at the peripheries of the feed rod and crystal. Since the surface tension of most molten semiconductors decreases as the temperature is increased, surface-tension variations due to the temperature variations drive two toroidal, axisymmetric cells of thermocapillary convection above and below the plane of the hottest circumference. Both cells involve free-surface flows toward a liquid–solid interface with axial return flows in the interior of the liquid. In the float-zone growth of alloyed crystals, the feed rod consists of a mixture of two unassociated semiconductors, and here we consider germanium with 10 at.% silicon, hereafter called GeSi, as an example [1]. Both species enter the liquid from the melting feed rod, and axial compositional variations develop in the liquid because there is rejection of one species during solidification at the crystal–melt interface. For our GeSi example, Si is preferentially absorbed into the crystal with the corresponding rejection of Ge into the liquid. For a steady state, the average composition of the crystal equals that of the feed rod, but the Si concentration in the liquid near the crystal–melt interface is much lower, and Si diffuses from its highest concentration at the feed-rod–melt interface to its lowest concentration at the crystal–melt interface. Since the surface tension increases as the Si concentration is increased, the surface-tension variation due to the compositional variation drives a single toroidal, axisymmetric cell of solutocapillary convection with a free-surface flow from the crystal toward the feed rod and with axial return flow in the interior of the

* Corresponding author. Tel.: +1-217-333-7979; fax: +1-217-244-6534.
E-mail address: jswalker@uiuc.edu (J.S. Walker).

0017-9310/02/$ - see front matter
PII: S0017-9310(02)00159-X

Nomenclature

b	length to diameter ratio of liquid bridge
B	magnetic flux density
C^*, C_0^*, C	dimensional, characteristic and dimensionless concentrations
D	diffusion coefficient
g	9.81 m/s^2
Ha	Hartmann number
N	interaction parameter
p	dimensionless pressure
Pe_g, Pe_m, Pe_t	crystal-growth, mass transport and thermal Peclet numbers
Pr	Prandtl number
r, θ, z	cylindrical coordinates with unit vectors $\hat{\mathbf{r}}$, $\hat{\theta}$, $\hat{\mathbf{z}}$
R	radius of liquid bridge
R_m	magnetic Reynolds number
t	dimensionless time
T_s^*, T	solidification and dimensionless temperatures
U, U_g	characteristic and crystal-growth velocities
$\mathbf{v}$	dimensionless velocity
$\alpha = Ha^{3/2}N^{-1}$	inertial parameter
β_T, β_C	thermal and solutal volumetric expansion coefficients
γ	surface tension
(ΔT^*)	temperature difference along free surface
κ	thermal diffusivity
λ_1, λ_2, λ_3	dimensionless parameters
μ, μ_p	dynamic viscosity and magnetic permeability
ρ	density
σ	electrical conductivity
ψ	Stokes stream function
ω	U_g/U

liquid. Above the hottest free-surface circumference, the thermocapillary and solutocapillary convections reinforce each other, but below this circumference, they tend to cancel each other. Since the density of the liquid mixture depends on temperature and composition, our model also includes the buoyant and solutal convections.

Recently 8 mm diameter GeSi crystals were grown by the float-zone process with an initially pure germanium melt and with a linear increase in the silicon concentration in the feed rod to 10 at.%. Patterns of the silicon distribution in the crystal indicated that the direction of the radial velocity near the crystal–melt interface was reversed when the silicon concentration exceeded a certain level, thus reflecting the emerging dominance of the solutocapillary convection over the local thermocapillary convection [1]. These crystals were grown without a magnetic field, but doped silicon crystals have been grown by the float-zone process with strong axial magnetic fields [2]. We do not know of any alloyed crystals which have been grown by the float-zone process with a strong axial magnetic field, so that our numerical predictions cannot be compared to any experimental measurements.

The objectives of this paper are to show: (1) that the competition between the solutocapillary and thermocapillary convections can lead to two different stable, steady, axisymmetric flows for certain parameter ranges, and (2) that the history of the process determines which of the two flows actually occurs. This paper uses a simplified model with a cylindrical free surface and with planar, isothermal liquid–solid interfaces, while the actual free surface sags due to the hydrostatic pressure, and the shapes of the actual liquid–solid interfaces depend on the global heat transfer and on the radial concentration variation. Our simplified model ignores some important phenomena, such as the periodic growth rate arising from the competition between the solutocapillary and thermocapillary convections [3]. The duality of flows for the same conditions will be altered by coupling with other phenomena in an actual crystal-growth process, but this duality will still occur for the reasons given here.

2. Problem formulation

The cylindrical free surface has a radius R, and the two planar liquid–solid interfaces are separated by $2bR$. We use cylindrical coordinates r, θ, z, with r and z normalized by R, with the z axis along the vertical centerline and with the origin at the center of the liquid. The dimensionless geometry is sketched in Fig. 1. In addition to the steady, uniform, axial magnetic field produced by a solenoid around the float-zone furnace, there is an induced magnetic field produced by the electric currents in the liquid. The characteristic ratio of the induced to applied magnetic fields is the magnetic Reynolds number $R_m = \mu_p \sigma U R$, where μ_p and σ are the magnetic permeability and electrical conductivity of the liquid, while U is a characteristic velocity. For U, we use the characteristic velocity for magnetically damped thermocapillary convection [4,5],

$$U = \frac{(-\partial\gamma/\partial T^*)(\Delta T^*)}{BR(\sigma\mu)^{1/2}}, \tag{1}$$

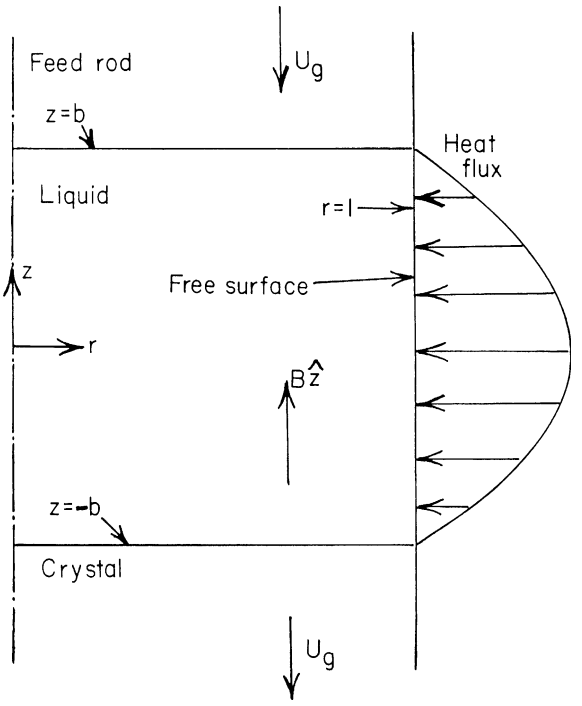

Fig. 1. Dimensionless geometry with a sinusoidal heat flux into the free surface, with a uniform axial magnetic field $B\hat{\mathbf{z}}$, and with a downward motion of the feed rod and crystal at the crystal-growth velocity U_g.

where γ and μ are the surface tension and dynamic viscosity of the liquid, while T^* is the dimensional liquid temperature and B is the magnetic flux density of the applied magnetic field. We assume that surface tension and density are both linear functions of T^* and of the concentration of silicon, C^*. For all crystal growth processes with steady magnetic fields, R_m is very small, so that it is appropriate to neglect the induced magnetic field.

In the conservation equation for internal energy, the characteristic ratio of the convective to conductive heat transfer is the thermal Peclet number $Pe_t = UR/\kappa$, where κ is the liquid's thermal diffusivity. Since U is proportional to B^{-1}, we assume that B is sufficiently large that convective heat transfer is negligible. We assume that the heat flux into the free surface at $r = 1$ varies sinusoidally from a maximum at $z = 0$ to 0 at $z = \pm b$. Then

$$T = \frac{I_0(\pi r/2b)}{I_0(\pi/2b)} \cos\left(\frac{\pi z}{2b}\right), \tag{2}$$

where $T = (T^* - T_s^*)/(\Delta T^*)$ and I_0 is the modified Bessel function of the first kind and zeroth order.

In the Navier–Stokes equation, the characteristic ratio of the electromagnetic (EM) body-force term to the inertial terms is the interaction parameter $N = \sigma B^2 R/\rho U$, where ρ is the density of molten germanium at T_s^*. Since N is proportional to B^3, we assume that B is sufficiently large that the inertial terms in the Navier–Stokes equation can be neglected. In order to estimate the error due to the neglect of inertial effects and convective heat transfer, we solved the complete Navier–Stokes and internal-energy equations for the half-zone problem with an axial magnetic field. The half-zone problem (1) has the same geometry as that presented in Fig. 1, (2) has no heat flux across the free surface at $r = 1$, (3) has a temperature difference of $2(\Delta T^*)$ between the two planar, isothermal liquid–solid interfaces at $z = \pm b$, and (4) includes thermocapillary convection, but does not include solutocapillary, buoyant or solutal convection. The half-zone problem is a benchmark for the experimental and numerical study of thermocapillary convection in the float-zone process [6–14], so that there are many numerical solutions to validate our solution of the complete equations without a magnetic field. In addition, Prange et al. [15] recently presented numerical solutions for the half-zone problem with a uniform axial magnetic field and provided thorough documentation of their numerical accuracy. They presented steady, axisymmetric solutions for a fixed value of (ΔT^*) and for $0 \leqslant Ha \leqslant 100$, where $Ha = BR(\sigma/\mu)^{1/2}$ is the Hartmann number. Our solution of the complete equations matches the results presented by Prange et al. [15].

We solved the complete equations for four values of Ha (100, 200, 400 and 800), for a wide range of values of N, for $b = 1$ and for a Prandtl number $Pr = \mu/\rho\kappa = 0.02$. Since $Pe_t = Pr\,Ha^2 N^{-1}$, both inertial effects and convective heat transfer become progressively more important as N is decreased. For each value of Ha, we began with the solution for $N = \infty$, and we used a continuation method suggested by Dr. Daniel Henry of L'Ecole Centrale de Lyon to obtain steady solutions for progressively smaller values of N. Morthland and Walker [5] showed that $\alpha = Ha^{3/2}N^{-1}$ is the correct parameter to represent inertial effects for a thermocapillary convection with a strong magnetic field which is parallel or nearly parallel to the free surface. The correct parameter is α rather than N because the dimensionless axial velocity inside a free-surface boundary layer is $O(Ha^{1/2})$ for large values of Ha. The ratio of the maximum velocity for a finite value of N to that for $N = \infty$ is plotted versus α for $Ha = 100$ and 200 in Fig. 2. The maximum velocity is always the axial velocity at some point along the free surface, while this maximum occurs at $z = 0$ for $N = \infty$ and moves toward the colder liquid–solid interface as N is decreased. We have also plotted ratios of maximum stream function, velocity at several points and temperature gradient at several points, and these other ratios are all closer to one for each value of α than those presented in Fig. 2. The curves for $Ha = 400$ and 800 are not presented in Fig. 2 because they are very close to the curve for $Ha = 200$. The results in Fig. 2

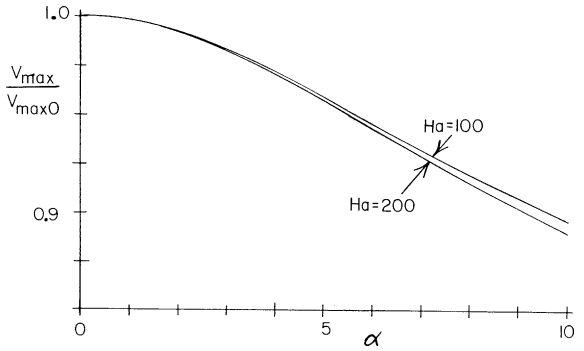

Fig. 2. For the half-zone problem with an axial magnetic field, the ratio of the maximum velocity to that for $\alpha = 0$ versus α for $Ha = 100$ and 200.

reveal the maximum errors associated with the neglect of inertial effects and of convective heat transfer for $Pr \leqslant 0.02$. The maximum errors are less than 1% and 3% for $\alpha \leqslant 2$ and $\alpha \leqslant 4$, respectively. In order to compute values of α and of other dimensionless parameters, we used the following properties: $\sigma = 1.5$ MS/m, $\rho = 5510$ kg/m^3, $\mu = 0.744$ mPa s, $\kappa = 0.175$ cm^2/s, $\partial\gamma/\partial T^* = -0.076$ mN/m K, $\partial\gamma/\partial C^* = 1.7$ mN/m at.%Si, $\beta_T = 5 \times 10^{-4}$ K^{-1}, $\beta_C = 5.43 \times 10^{-3}$ (at.%Si)$^{-1}$, $R = 4$ mm and $(\Delta T^*) = 6$ K, where β_T and β_C are the thermal and solutal volumetric expansion coefficients. With these values, $\alpha = 2$ and 4 correspond to $B = 2.4$ and 1.5 T, respectively.

For an axisymmetric flow, the radial velocity and the axial magnetic field produce an azimuthal electric current which interacts with the magnetic field to produce an EM body force opposing the radial velocity. The dimensionless, inertialess Navier–Stokes equation is

$$0 = -\nabla p + Ha^{-1}(\lambda_1 T + \lambda_2 C)\hat{\mathbf{z}} - v_r \hat{\mathbf{r}} + Ha^{-2}\nabla^2 \mathbf{v}, \qquad (3)$$

where p is the deviation of the pressure from the uniform-density hydrostatic pressure normalized by $\sigma U B^2 R$, $C = C^*/C_0^*$ is the silicon concentration normalized by the uniform concentration C_0^* in the feed rod, $\mathbf{v} = v_r\hat{\mathbf{r}} + v_z\hat{\mathbf{z}}$ is the velocity normalized by U, and $\hat{\mathbf{r}}, \hat{\theta}, \hat{\mathbf{z}}$ are unit vectors for the cylindrical coordinates. The dimensionless parameters are

$$\lambda_1 = \frac{\rho g \beta_T R^2}{(-\partial\gamma/\partial T^*)}, \quad \lambda_2 = \frac{\rho g \beta_C C_0^* R^2}{(-\partial\gamma/\partial T^*)(\Delta T^*)}, \qquad (4a, b)$$

We introduce the Stokes stream function $\psi(r,z)$ in order to satisfy the continuity equation, where

$$v_r = \frac{1}{r}\frac{\partial\psi}{\partial z}, \quad v_z = -\frac{1}{r}\frac{\partial\psi}{\partial r}. \qquad (5a, b)$$

Section 3 presents solutions for $Ha = 100$, 200 and 400. In the asymptotic solution for $Ha \gg 1$, the liquid bridge is divided into: (a) an inviscid core region, (b) Hartmann layers with $O(Ha^{-1})$ thickness between the core and the liquid–solid interfaces at $z = \pm b$, (c) a parallel layer with $O(Ha^{-1/2})$ thickness adjacent to the free surface at $r = 1$, and (d) intersection regions with $\Delta r = O(Ha^{-1/2})$ and $\Delta z = O(Ha^{-1})$ between the parallel layer and the liquid–solid interfaces at $z = \pm b$. For $Ha = 100$, the Hartmann layers and intersection regions are very thin and have a simple, local, exponential structure [16], but the parallel layer occupies approximately $0.4 < r < 1.0$, so it is definitely not thin. Therefore the formal asymptotic solution for $Ha \gg 1$, which assumes that the parallel layer is vanishingly thin, is not appropriate for the Hartmann number range considered here. However there is no need to numerically reproduce the simple exponential structure of the Hartmann layers and intersection regions, since their large-Ha analytical solutions are certainly valid for $Ha = 100$. Therefore we use a composite core-parallel-layer solution [17] where we neglect terms in Eq. (3) which are negligible in both the core and parallel layer, and we apply Hartmann conditions at $z = \pm b$. The terms in Eq. (3) which are negligible are all the viscous terms in the r component of Eq. (3) and the term $Ha^{-2}\partial^2 v_z/\partial z^2$ in the z component. The Hartmann layers and intersection regions match any radial velocity in the composite core-parallel-layer solution, provided v_z in this solution satisfies the Hartmann conditions [16]. Neglecting $O(Ha^{-1})$ terms, these conditions are that $v_z = 0$ at $z = \pm b$, so that the error in our composite solution is $O(Ha^{-1})$.

The equation governing the stream function for the composite solution is

$$\frac{\partial^4\psi}{\partial r^4} - \frac{2}{r}\frac{\partial^3\psi}{\partial r^3} + \frac{3}{r^2}\frac{\partial^2\psi}{\partial r^2} - \frac{3}{r^3}\frac{\partial\psi}{\partial r} - Ha^2\frac{\partial^2\psi}{\partial z^2} = Ha\lambda_1 r\frac{\partial T}{\partial r} + Ha\lambda_2 r\frac{\partial C}{\partial r}. \qquad (6)$$

The boundary conditions at $z = \pm b$ are $\psi = 0$, and those at $r = 1$ are

$$\frac{\partial^2\psi}{\partial r^2} - \frac{\partial\psi}{\partial r} = Ha\frac{\partial T}{\partial z} - Ha\lambda_3\frac{\partial C}{\partial z}, \quad \psi = 0, \qquad (7a, b)$$

where the dimensionless parameter

$$\lambda_3 = \frac{(\partial\gamma/\partial C^*)C_0^*}{(-\partial\gamma/\partial T^*)(\Delta T^*)}. \qquad (8)$$

The change in the dimensionless concentration along the free surface is $(\Delta C)_{fs} = C(1,b) - C(1,-b)$, so that $\lambda_3(\Delta C)_{fs}$ is a characteristic ratio of the solutocapillary to thermocapillary convections. The appropriate condition at the centerline is that the Taylor series for ψ has only even powers of r, starting with r^2.

The equation governing the dimensionless concentration of silicon in the liquid is

$$\frac{1}{r}\frac{\partial\psi}{\partial z}\frac{\partial C}{\partial r}-\left(\omega+\frac{1}{r}\frac{\partial\psi}{\partial r}\right)\frac{\partial C}{\partial z}=Pe_{\mathrm{m}}^{-1}\left(\frac{\partial^2 C}{\partial r^2}+\frac{1}{r}\frac{\partial C}{\partial r}+\frac{\partial^2 C}{\partial z}\right), \tag{9}$$

where the dimensionless parameters are $\omega = U_{\mathrm{g}}/U$ and the mass transport Peclet number $Pe_{\mathrm{m}} = UR/D$, while U_{g} is the crystal-growth velocity, i.e., the rate at which the feed rod melts and the crystal grows, and D is the diffusion coefficient for silicon in molten germanium. The boundary conditions are

$$\frac{\partial C}{\partial r}=0, \quad \text{at } r=1, \tag{10a}$$

$$C+Pe_{\mathrm{g}}^{-1}\frac{\partial C}{\partial z}=1, \quad \text{at } z=b, \tag{10b}$$

$$\frac{\partial C}{\partial z}+Pe_{\mathrm{g}}(1-k_{\mathrm{s}})C=0, \quad \text{at } z=-b, \tag{10c}$$

where $Pe_{\mathrm{g}} = U_{\mathrm{g}}R/D = \omega Pe_{\mathrm{m}}$ is the crystal-growth Peclet number, and k_{s} is the segregation coefficient which is the ratio of the silicon concentration in the crystal at a point on the crystal–melt interface to that in the melt at the same point. The Taylor series for C consists of even powers of r.

We used a Chebyshev spectral collocation method and a Newton–Raphson iterative method to solve for ψ and C. For each case, we increased the number of radial and axial Gauss–Lobatto collocation points until the results did not change.

3. Results

We present a parametric study with variations of Ha and Pe_{m}, and with fixed values of the other parameters. The values of the other parameters are: $b = 1$, $\lambda_1 = 5.69$, $\lambda_2 = 103$, $\lambda_3 = 37.3$, $Pe_{\mathrm{g}} = 0.0926$, and $k_{\mathrm{s}} = 4.2$, which correspond to the properties listed in Section 2, plus $C_0^* = 10$ at.%Si and $U_{\mathrm{g}} = 0.5$ mm/h.

For $Pe_{\mathrm{m}} = Ha = 100$, there are two stable, steady, axisymmetric solutions. We used a time integration to obtain the first solution. We added $\partial C/\partial t$ to the left side of Eq. (9), where t is time normalized by R/U. We began with $C = 0$ at $t = 0$. For an initial period, we replaced the one on the right side of Eq. (10b) with a linear function of t from zero to one. For this time integration, the thermocapillary and buoyant convections always exist, and the solutocapillary and solutal convections are added as silicon enters the liquid from the melting feed rod. This time integration approaches a steady-state solution which we call the TC solution because the thermocapillary convection remains dominant over the lower part of the free surface where it competes with the solutocapillary convection.

The streamlines and contours of constant C for the TC solution for $Pe_{\mathrm{m}} = Ha = 100$ are presented in Fig. 3. Relative to the flow with only the thermocapillary and buoyant convections, the addition of the solutocapillary and solutal convections has increased the strength of the upper circulation by 11.9%, has decreased the strength of the lower circulation by 37.4% and has moved the free-surface stagnation point from $z = 0$ to -0.4. The only significant values of $\partial C/\partial z$ at $r = 1$ are located near the free-surface stagnation point, while the free-surface convective mass transport in the two capillary circulations essentially eliminates the free-surface concentration gradient for $z > 0.0$ and $z < -0.6$.

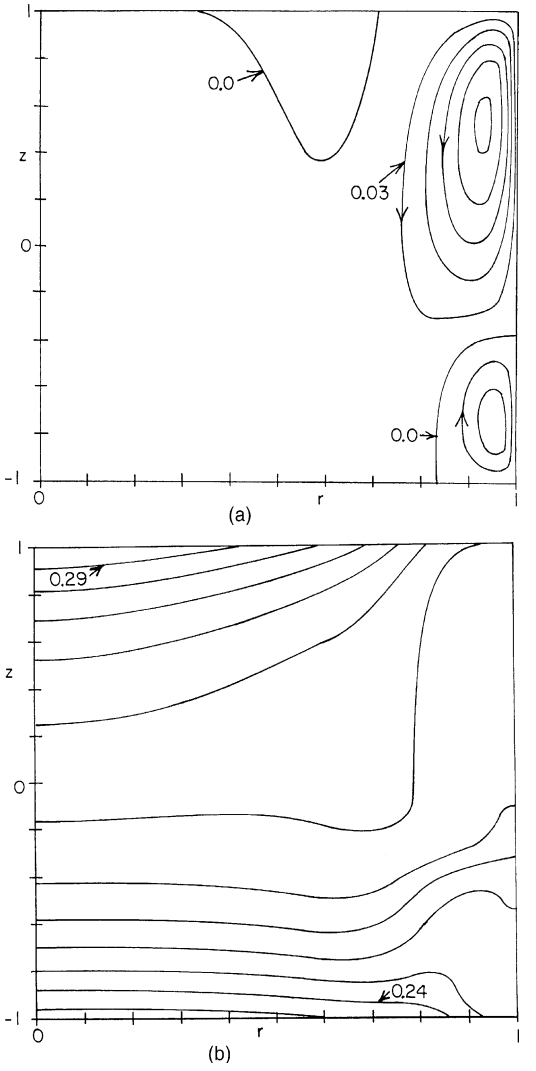

Fig. 3. TC solution for $Ha = Pe_{\mathrm{m}} = 100$. (a) Streamlines: $\psi = 0.03k$, for $k = -2$ to 5. (b) Constant concentration contours: $C = 0.235 + 0.005k$, for $k = 0$ to 11.

We used continuation through a series of steady-state solutions for $Ha = 100$ and for Pe_m increasing from 1 to 100 to obtain the second stable, steady, axisymmetric solution. For $Pe_m = 1$, the contours of constant C are nearly horizontal and are very close to those with only diffusion and a uniform downward velocity of U_g, so that there is the largest possible free-surface concentration gradient for this growth rate. The solutocapillary convection overwhelms the thermocapillary convection, and there is a single circulation with flow along the entire free surface from the crystal toward the feed rod. As Pe_m is increased from 1 to 100, convective mass transport reduces the free-surface concentration gradient, so that the maximum value of ψ decreases by 70.5%, but v_z remains positive over the entire free surface. We call the solution obtain by this continuation the SC solution because the solutocapillary convection remains dominant over the lower part of the free surface where it competes with the thermocapillary convection.

The streamlines and contours of constant C for the SC solution for $Pe_m = Ha = 100$ are presented in Fig. 4. The contours of constant C in Figs. 3b and 4b are similar except in the region $0.7 < r < 1.0$ and $-1.0 < z < -0.5$. For Fig. 3b, the thermocapillary convection existed before the solutocapillary convection was added with a constant value of Pe_m, so that the convective mass transport for $z < -0.5$ prevented the development of a local free-surface concentration gradient and thus prevented the solutocapillary convection from overwhelming the thermocapillary convection. For Fig. 4b, the thermocapillary and solutocapillary convections always coexisted, starting with negligible convective mass transport for $Pe_m = 1$ with its large free-surface concentration gradient and with the associated dominance by the solutocapillary convection. As Pe_m was increased, the established free-surface concentration gradient kept a balance between the thermocapillary and solutocapillary convections, so that there continued to be little convective mass transport for $z < -0.5$, leading to a larger local free-surface concentration gradient.

We used the same continuation method to study changes in both the SC and TC solutions as Pe_m is varied for $Ha = 100$. We have already discussed the SC solution for $Pe_m \leqslant 100$. When Pe_m is increased from 100 for the SC solution, a small region of clockwise circulation with $\psi < 0$ appears near $r = 1$ and $z = -0.5$ at $Pe_m = 120$, reflecting the first point where the thermocapillary convection overtakes the solutocapillary convection. The free-surface temperature gradient is largest at $z = -1$, but the free-surface concentration gradient is also large here, so that solutocapillary convection continues to dominate near the crystal–melt interface. At $z = -0.5$, the temperature gradient is smaller, but the concentration gradient is much smaller due to the convective mass transport associated with the single circulation, so that this is the location where the clockwise thermocapillary convection first emerges. As Pe_m is increased from 120, the strength of the clockwise circulation increases, this circulation remains in the region $0.9 < r < 1.0$ and $-0.65 < z < -0.3$, with the stronger counterclockwise circulation going around it. The steady SC solution does not exist for $Pe_m > 181$. If we use the steady SC solution for $Pe_m = 181$ as the initial condition for a time integration with $Pe_m = 182$, the small clockwise circulation near $z = -0.5$ grows in strength and extends toward $z = -1$. The associated downward convective mass transport decreases the free-surface concentration gradient for $z < -0.4$, thus reducing the local solutocapillary convection and allowing the emerging dominance of the thermocapillary convection. This time

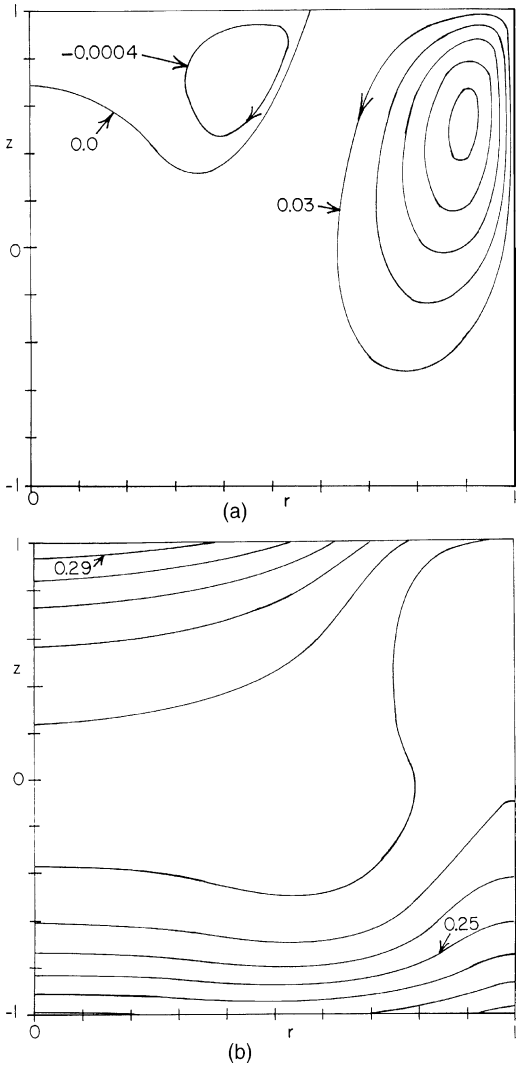

Fig. 4. SC solution for $Ha = Pe_m = 100$. (a) Streamlines: $\psi = 0.03k$, for $k = 0$ to 5 and $\psi = -0.0004$. (b) Constant concentration contours: $C = 0.235 + 0.005k$, for $k = 0$ to 11.

integration approaches the steady TC solution for $Pe_m = 182$.

For the steady TC solution, as Pe_m is decreased from 100 to 80 for $Ha = 100$, the strength of the clockwise circulation near the crystal–melt interface decreases. The steady TC solution does not exist for $Pe_m < 80$. If the steady TC solution for $Pe_m = 80$ is used as the initial condition for a time integration with $Pe_m = 79$, the clockwise circulation for $-1.0 < z < -0.4$ decreases in strength and in axial extent. The associated reduction in convective mass transport permits a free-surface concentration gradient to develop for $z < -0.4$, so that the growing solutocapillary convection eventually eliminates the local clockwise circulation, and the solution approaches the steady SC solution for $Pe_m = 79$.

In summary for $Ha = 100$, the only steady solution for $Pe_m < 80$ is the SC solution, and the only steady solution for $Pe_m > 181$ is the TC solution. For $80 \leqslant Pe_m \leqslant 181$, both the SC and TC solutions are possible. For the parameter range where both may occur, which of the two solutions actually occurs in a particular crystal-growth process depends on the history of the process, as illustrated by the ways we found the two solutions. For processes with a constant magnetic field strength, the thermocapillary convection is established first when the feed rod is melted, and the solutocapillary convection is added later as crystal growth begins and rejection of one species creates an axial concentration gradient. Such a constant field strength process would always lead to the TC solution in the overlap range because the initial thermocapillary convection would prevent the development of the free-surface concentration gradient near the crystal–melt interface. On the other hand, the steady SC solution in the overlap range could be obtained by first increasing the magnetic field strength after the start of crystal growth in order to suppress convective mass transport enough to permit development of a free-surface concentration gradient and the associated dominance of the solutocapillary convection. Then the field strength could be reduced and the SC solution would persist throughout the overlap range.

For $Ha = 200$, both TC and SC solutions exist for $90.5 \leqslant Pe_m \leqslant 220$, and for $Ha = 400$, both solutions exist for $123 \leqslant Pe_m \leqslant 300$. The basic characteristics of the two solutions do not change significantly as Ha is increased from 100 to 800, except that the circulations are confined to a layer adjacent to the free surface whose radial extent decreases as $Ha^{-1/2}$, as expected [5].

4. Concluding remarks

This paper demonstrates that, for each value of the Hartmann number, there is a range of values of the mass transport Peclet number for which two stable, steady, axisymmetric flows are possible. For the parameter range with two possible steady solutions, the history of the process determines which of the two solutions actually occurs. If the solutocapillary convection is added to an existing thermocapillary convection, then the convective mass transport associated with the thermocapillary convection prevents the development of the free-surface concentration gradient needed to drive a solutocapillary convection that can overwhelm the thermocapillary convection. Thus the thermocapillary convection remains dominant. On the other hand, if the convective mass transport is suppressed after both the thermocapillary and solutocapillary convections exist, for example, by briefly increasing the magnetic field strength, then the free-surface concentration gradient is established. When strong convective mass transport resumes, the established free-surface concentration gradient drives a solutocapillary convection which cancels the local thermocapillary convection, so that there is little local convective mass transport and the solutocapillary convection remains dominant.

We have not investigated the possibility of two different steady, axisymmetric flows in the float-zone process without a magnetic field because the flow is unsteady and nonaxisymmetric in every actual float-zone crystal-growth process without a magnetic field. Even for the float-zone growth of 8 mm diameter silicon crystals in a uniform axial magnetic field with $B = 0.5$ T, the flow remains unsteady and nonaxisymmetric [18,19]. Therefore we have only considered strong magnetic fields, such as those used by Cröll et al. [2] for growth of doped silicon crystals.

Acknowledgements

This research was supported by the US National Aeronautics and Space Administration under Grants NAG8-1453 and NAG8-1705. The calculations were performed on a workstation donated by the International Business Machines Corporation.

References

[1] T.A. Campbell, M. Schweizer, P. Dold, A. Cröll, K.W. Benz, Float-zone growth of $Ge_{1-x}Si_x$ ($x \leqslant 10$ at.%) single crystals, J. Cryst. Growth 226 (2001) 231–239.

[2] A. Cröll, F.R. Szofran, P. Dold, K.W. Benz, S.L. Lehoczky, Floating-zone growth of silicon in magnetic fields. II. Strong static axial fields, J. Cryst. Growth 183 (1998) 554–563.

[3] D. Schwabe, X. Da, A. Scharmann, Unstable flow and solidification speed due to the interaction of thermocapillary and solutocapillary forces in directional solidification, J. Cryst. Growth 166 (1996) 483–488.

[4] Y.Y. Khine, J.S. Walker, Thermocapillary convection in a cylinder with a strong nonuniform axisymmetric magnetic field, J. Fluid Mech. 276 (1994) 369–388.
[5] T.E. Morthland, J.S. Walker, Convective heat transfer due to thermocapillary convection with a strong magnetic field parallel to the free surface, Int. J. Heat Mass Transfer 40 (14) (1997) 3283–3291.
[6] D. Schwabe, A. Scharmann, F. Preisser, R. Oeder, Experiments on surface tension driven flow in floating zone melting, J. Cryst. Growth 43 (1978) 305–312.
[7] Y. Shen, G.P. Neitzel, D.F. Jankowski, H.D. Mittelmann, Energy stability of thermocapillary convection in a model of the float-zone crystal-growth process, J. Fluid Mech. 217 (1990) 639–660.
[8] R. Velten, D. Schwabe, A. Scharmann, The periodic instability of thermocapillary convection in cylindrical liquid bridges, Phys. Fluids A 3 (2) (1991) 267–279.
[9] H.C. Kuhlmann, H.J. Rath, Hydrodynamic instabilities in cylindrical thermocapillary liquid bridges, J. Fluid Mech. 247 (1993) 247–274.
[10] M. Wanschura, V.M. Shevtsova, H.C. Kuhlmann, H.J. Rath, Convective instability mechanisms in thermocapillary liquid bridges, Phys. Fluids 7 (5) (1995) 912–925.
[11] H.C. Kuhlmann, M. Wanschura, V. Shevtsova, H.J. Rath, Energy analysis of some flow instabilities in liquid bridges, Adv. Space Res. 16 (7) (1995) 15–22.
[12] R. Savino, R. Monti, Three-dimensional numerical simulations of thermocapillary instabilities in floating zones, Appl. Sci. Res. 56 (1996) 19–41.
[13] G. Chen, A. Lizée, B. Roux, Bifurcation analysis of the thermocapillary convection in cylindrical liquid bridges, J. Cryst. Growth 180 (1997) 638–647.
[14] J. Leypoldt, H.C. Kuhlmann, H.J. Rath, Three-dimensional numerical simulation of thermocapillary flows in cylindrical liquid bridges, J. Fluid Mech. 414 (2000) 285–314.
[15] M. Prange, M. Wanschura, H.C. Kuhlmann, H.J. Rath, Linear stability of thermocapillary convection in cylindrical liquid bridges under axial magnetic fields, J. Fluid Mech. 394 (1999) 281–302.
[16] J.S. Walker, G.S.S. Ludford, J.C.R. Hunt, Three-dimensional MHD duct flows with strong transverse magnetic fields. Part 3. Variable-area rectangular ducts with insulating walls, J. Fluid Mech. 56 (1) (1972) 121–141.
[17] N. Ma, J.S. Walker, A model of dopant transport during Bridgman crystal growth with magnetically damped buoyant convection, J. Heat Transfer 122 (2000) 159–164.
[18] A. Cröll, P. Dold, K.W. Benz, Segregation in Si floating-zone crystals grown under microgravity and in a magnetic field, J. Cryst. Growth 137 (1994) 95–101.
[19] P. Dold, A. Cröll, K.W. Benz, Floating-zone growth of silicon in magnetic fields. I. Weak static axial fields, J. Cryst. Growth 183 (1998) 545–553.